World Academy of Science, Engineering and Technology
International Journal of Electrical and Computer Engineering
Vol:4, No:4, 2010

Effective Design Parameters on the End Effect in Single-Sided Linear Induction Motors

A. Zare Bazghaleh, M. R. Naghashan, H. Mahmoudimanesh, M. R. Meshkatoddini

***Abstract*—**Linear induction motors are used in various industries but they have some specific phenomena which are the causes for some problems. The most important phenomenon is called end effect. End effect decreases efficiency, power factor and output force and unbalances the phase currents. This phenomenon is more important in medium and high speeds machines. In this paper a factor, *EEF* , is obtained by an accurate equivalent circuit model, to determine the end effect intensity. In this way, all of effective design parameters on end effect is described. Accuracy of this equivalent circuit model is evaluated by two dimensional finite-element analysis using ANSYS. The results show the accuracy of the equivalent circuit model.

***Keywords*—**Linear induction motor, end effect, equivalent circuit model, finite-element method.

I. Introduction

NOWADAYS the applications of linear motors (LMs) are widely extended. [1],[2]. LMs can provide linear motion directly. Thus there is no need to wheel, gear or any type of rotary to linear motion convertors. Thanks to absence of mechanical convertors, this type of motor has good performance and high reliability [3].

From different type of LMs the linear induction motors (LIMs) are used more, specially, in the form of single-sided linear induction motors (SLIMs). In some applications of SLIMs, the secondary is cage-type or wounded [4]. But by using of a high conducting plate Backed by a ferromagnetic material (Back iron), instead of cage or wounded type of secondary, the structure of SLIM will be more and more simplified. This is because of widely usage of SLIM. Several different methods have been presented for analysis of LIMs, such as equivalent circuit model (ECM), 1-D and 2-D electromagnetic field analysis and numerical methods including finite-element (FEM) and finite-difference (FDM) methods [5]-[9].

End effect of LIMs has been so far studied in several researches, in which different purposes have been considered. N. Fujii and T. Harada have studied end effect in SLIM with ladder type secondary. They presented t_p/t_s as a factor to measure the degree of end effect [10]. Where in which t_p is passing duration of primary core at a secondary point and t_s half-period of slip frequency. In another paper the end effect has been investigated completely by using of FEM [11]. This phenomenon is baneful and affects the output of motor thus it is a good idea to compensate this phenomenon in LIMs [12]. But it is a better idea to design a machine with lower degree of end effect. To achieve this purpose it is necessary to reconnoiter all of effective design parameters on end effect. In a research, some of these parameters are introduced by help of 1-D electromagnetic field analysis [13].

In this paper all of effective design parameters will be described. In order to perform this idea, a suitable ECM will be introduced. This model is obtained by modifying the Duncan's model. The resultant ECM includes end effect, truly. By help of this ECM a factor will be obtained which describes the end effect intensity. Then the effect of design parameters on the end effect will be investigated through appropriate 3-plots by help of MATLAB. Finally, the 2-D time stepping nonlinear FEM is carried out by help of ANSYS to evaluate the proffered ECM.

II. ECM of SLIMs Considers End Effect

The relative motion between short primary and long secondary, causes to end effect. This effect leads to braking force and additional loss that are produced by eddy currents at the entry and exit rail as it can be seen in Fig.1 [14].

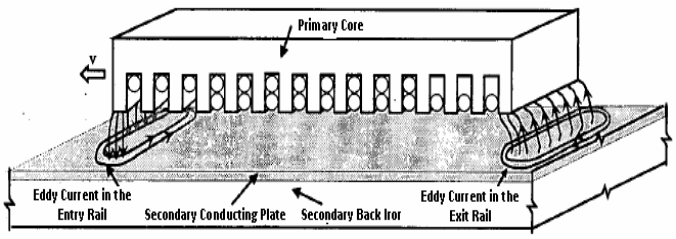

Fig. 1 Eddy current generation at the entry and exit rail

As it can be seen in Fig.2, by neglecting end effect, the ECM of SLIM comes to ECM of rotary induction motor (RIM) [2].

A. Zare Bazghaleh, Power and Water University of Technology, Tehran, Iran (corresponding author to provide phone: 09376328332; e-mail: amir.zarebazghaleh27@gmail.com).

M. R. Naghashan, Power and Water University of Technology, Tehran, Iran. (e-mail: naghashan@yahoo.com).

H. Mahmoudimanesh, Claude Bernard Lyon 1 University, Lyon, France (e-mail: mahmoudimanesh@yahoo.com).

M. R. Meshkatoddini, Power and Water University of Technology, Tehran, Iran (e-mail: meshkatoddini@ieee.org).

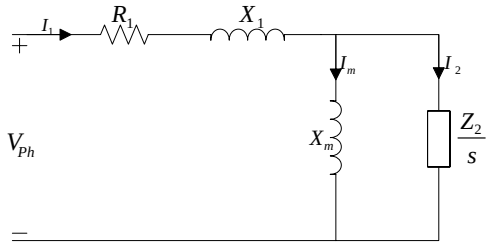

Fig. 2 ECM of SLIM by neglecting end effect

One of the best ECMs that included end effect is the ECM suggested by Duncan [15]. In this section Duncan's ECM has been described and modified to achieve the suitable ECM, for a fast and accurate study on SLIM.

The rise and decay of secondary eddy current are controlled by the secondary leakage time constant $T_{lr} = L_{lr}/R_2$ and total secondary time constant $T_r = L_r/R_2$, respectively. Noting that the entry eddy current caused by entry end effect decays with the time constant T_r, the average value of entry eddy current i_ε^e over the motor length is given by:

$$i_\varepsilon^e = \frac{I_m}{T_\upsilon}.\int_0^{T_\upsilon} e^{-t/T_r}dt \tag{1}$$

Where T_v is the time that the motor needs to overpass a point. Motor can transverse a distance equal to $v.T_r$ over the time duration T_r. Thus, the motor length can be normalized by $v.T_r$ such that [15]:

$$Q = \frac{l_S\ R_2}{(L_2 + L_m)v} \tag{2}$$

By this way, the normalized motor length depends on velocity. Using (2), equation (1), becomes:

$$i_\varepsilon^e = \frac{I_m}{Q}.\int_0^{Q} e^{-x}\,dx = I_m\frac{1-e^{-Q}}{Q} \tag{3}$$

Thus, the magnetizing current reduces as following:

$$I_m - i_\varepsilon^e = I_m\left[1-\frac{1-e^{-Q}}{Q}\right] \tag{4}$$

The reduction in the magnetizing current will be accounted in ECM by modifying the magnetizing inductance as following:

$$L_m{}' = L_m(1-\frac{1-e^{-Q}}{Q}) \tag{5}$$

But that will not be all. Because, when induced eddy current circulates in secondary plats, it causes to ohmic loss. This loss will be produced by R_2.The effective value of eddy current over the motor length can be evaluated as:

$$i_{\varepsilon rms} = \left[\frac{I_m{}^2}{Q}\int_0^{Q} e^{-2x}dx\right]^{1/2} = I_m\left[\frac{1-e^{-2Q}}{2Q}\right]^{1/2} \tag{6}$$

Therefore, the value of ohmic loss due to entry eddy current can be obtained by:

$$P_{entry} = i_{\varepsilon rms}^2 R_2 = I_m{}^2.R_2\frac{1-e^{-2Q}}{2Q} \tag{7}$$

The total eddy current in the air gap can be obtained from (3) as $I_m(1-e^{-Q})$. To satisfy the steady state condition in the air gap, eddy current must be vanished at exit rail during the time T_v. Therefore, the ohmic loss caused by exit eddy current may be evaluated by:

$$P_{exit} = \frac{L_r I_m{}^2(1-e^{-Q})^2}{2T_\upsilon} = I_m^2\frac{(1-e^{-Q})^2}{2Q} \tag{8}$$

Thus, from (7) and (8), the total ohmic loss due to eddy current in the secondary will be:

$$P_{eddy} = I_m^2 R_2\frac{1-\exp(-Q)}{Q} \tag{9}$$

As it can be seen in equation (9), this ohmic power loss can be represented by a resistor which is connected in series to the magnetizing inductance.

As it can be seen in Fig.3, the difference between Duncan model and conventional equivalent circuit of RIM is the change in the magnetizing branch due to the end effect [2].

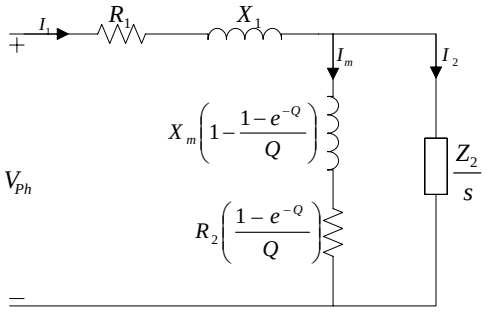

Fig. 3 ECM suggested by Duncan

In Duncan model The ECM parameters are obtained by the standard open and short circuit test, but, because of the specific phenomena in LIMs, the ECM parameters change with slip and cannot be obtained by standard tests [3]. The best way to obtain ECM parameters of SLIM, is using analytical equations [16],[17].

$$R_1 = \frac{1}{\sigma_{cu}}\left(\frac{2W_s + 2L_{ce}}{N_{ph}I}\right)J_c N_{ph}{}^2 \tag{10}$$

$$X_1 = \frac{2\mu_0\omega}{p}\left[\left(\lambda_s\left(1+\frac{3}{2p}\right)+\lambda_d\right)\frac{W_s}{q}+\lambda_e l_{ce}\right] \tag{11}$$

$$Z_{cp}(s) = (js\omega\mu_o/K_{cp})\left[1/\tanh(K_{cp}d)\right] \times K_{tr}W_{se}/\tau \tag{12}$$

$$Z_{Fe}(s) = \left(js\omega\mu_{Fe}/K_{Fe}\right)\left[1/\tanh(K_{Fe}d_{iron})\right] \times K_{tr}W_{se}/\tau \tag{13}$$

$$X_m = \left[4m_1\mu_o f(N_{ph}K_w)^2/\pi\ p\right]\times W_{se}\tau/g_{ei} \tag{14}$$

The secondary core in SLIMs is made of solid iron or steel, so, saturation occurs in some operation conditions. In order to

take this effect into account, the saturation coefficient, K_s, has been defined and causes to increase in air gap length.

$$g_{ei} = K_l K_c (1 + K_s)(g_m + d) \quad (15)$$

The saturation coefficient for the secondary back iron, K_s, is the ratio of back iron reluctance to the sum of conductor and the air gap reluctance. Considering the average length of solid back iron flux path to be $1/\beta$ and the depth of field penetration in the iron as δ_i, the saturation factor takes the form [2]:

$$K_s = \frac{\mu_i}{\mu_0 \delta_i (g_m + d) K_c \beta^2} \quad (16)$$

$$\delta_i = \mathrm{Re}\left[1/(\beta^2 + j\omega\mu_i s\sigma_{1e})^{0.5}\right] \quad (17)$$

The average permeability of back iron can be computed during an iterative procedure [18]. In order to obtain this goal first it is necessary to calculate the approximate value of flux density in the air gap [2].

$$B_{ag} = jJ_m\mu_0 / \left[g_{ei}\beta(1 + jsG_e)\right] \quad (18)$$

$$J_m = \sqrt{2} m N_{ph} K_w I / p\tau \quad (19)$$

Assuming an exponential form for the field distribution in the back iron the flux density at the surface of the back iron takes the form [2]:

$$B_{si} = |B_{ag}| / \delta_i \beta \quad (20)$$

The secondary of SLIMs has no specific paths for induced currents. The phenomenon cause to increase in equivalent secondary resistance. This effect is known as the transverse edge effect and should be considered by suitable coefficients [2].

$$\sigma_{1e} = \sigma_{fe} / k_{fe} \quad (21)$$

$$\sigma_{2e} = \sigma_{cp} \times k_{cp} \quad (22)$$

A realistic air gap flux density lower than 0.4T, leads to moderate flux densities in the primary core iron, and thus core losses can be neglected and the propulsion force, the power factor, and the efficiency can be obtained from [18]:

$$F_x = 3{I_2}^2 R_2 / s \quad (23)$$

$$\cos\varphi = \left(F_x 2 f\tau + 3I^2 R_1 + 3I_m^2 R_2 \frac{1 - e^{-Q}}{Q}\right) / 3VI \quad (24)$$

$$\eta = F_x 2 f\tau (1 - s) / \left(F_x 2 f\tau + 3I^2 R_1 + 3I_m^2 R_2 \frac{1 - e^{-Q}}{Q}\right) \quad (25)$$

III. End Effect Intensity

Two ECMs are described in last section. The first one (Fig.2) does not consider end effect but the second one (Fig.3) considers the additional loss in the entry and exit rail and reduction of force caused by end effect.

Therefore, the air gap power which is calculated by the first ECM at constant current, $P_{ag(ne)}$, is for a SLIM which has no end effect, But the air gap power which is calculated by the second ECM, $P_{ag(we)}$, contains the additional loss and force reduction caused by end effect. Thus, end effect intensity, *EEF* , can be measured by the following equation:

$$EEF = \frac{P_{ag(ne)} - P_{ag(we)}}{P_{ag(ne)}} = 1 - \frac{P_{ag(we)}}{P_{ag(ne)}} \quad (26)$$

EEF versus motor speed is shown in Fig.4.

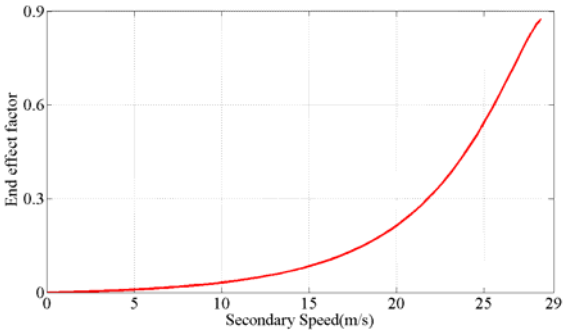

Fig. 4 EEF versus motor speed

IV. Effective Design Parameters

TABLE I
Main Design Parameters of Case Study SLIM

Symbol	Value
Number of poles	4
Number of slots per pole per phase	2
Nominal speed (m/s)	20
Nominal current (A)	200
Pole pitch (m)	0.28
Frequency (Hz)	60
Primary width (m)	0.36
Current density (A/mm^2)	6.5
Slip	0.3
Air gap length (mm)	3
Conducting plate thickness (mm)	1
Conducting plate resistivity to aluminum resistivity ratio	0.6

The EEF can be used to discover the effective design parameters on the end effect intensity. In this section the influence of design parameters on end effect intensity will be described. To achieve this goal the described ECM will be used. The case study machine simulation detail has been described in Table I.

Change in the air gap length can affect the flux distribution in the air gap and secondary. By this way, an increase in the air gap length increases the loss in the exit and entry area of rail. Also, in the case of nonferrous conducting plate, if the conducting plate thickness increases, the secondary time constant increase that lead to end effect travelling wave of smaller magnitude. As it can be seen in Fig.5, EEF increases by increasing the air gap length and decreasing the secondary conducting plate thickness.

Variation of end effect intensity, with the secondary conducting plate resistivity and slot pitch to slot width ratio (SPSW), is justifiable by the time constant of secondary, too. A conducting plate with larger resistivity caused to smaller secondary time constant. It leads to a more intensive end effect. Variations in the stator core design can affect the end effect intensity, too. Larger amount of SPSW (smaller tooth

width) causes to larger secondary leakage reactance and larger secondary time constant. Finally, it results end effect travelling wave of smaller magnitude. Fig.6 shows the variation of EEF related to SPSW and conducting plate resistivity to aluminum resistivity ratio (CRAR).

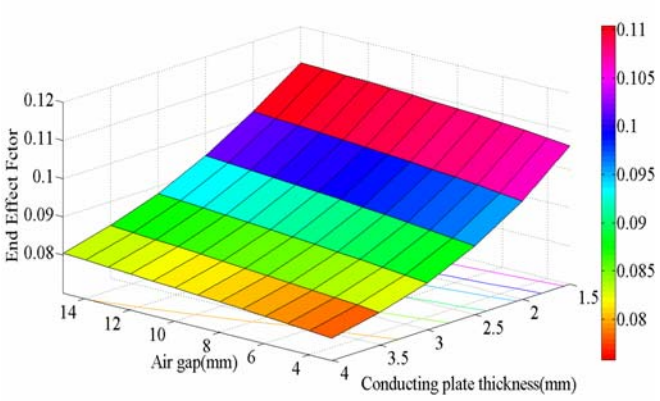

Fig. 5 End effect Intensity versus air gap length and conducting plate thickness

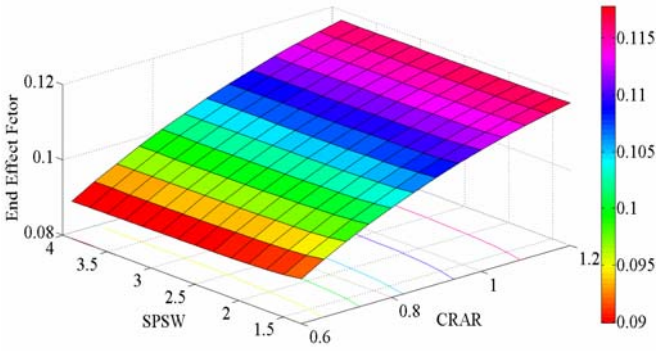

Fig. 6 End effect Intensity versus slot pitch to slot width ratio and conducting plate resistivity to aluminum resistivity ratio

Fig.7 shows the variation of EEF related to the number of pole pairs (NP) and number of slots per pole per phase (NSPP). The decrease in the EEF with increase in NP caused by this fact, more poles tend to share the constant end effect loss between them. It is seen that NSPP has no sensible effect on the EEF, but larger NSPP can moderate the phases unbalance due to end effect.

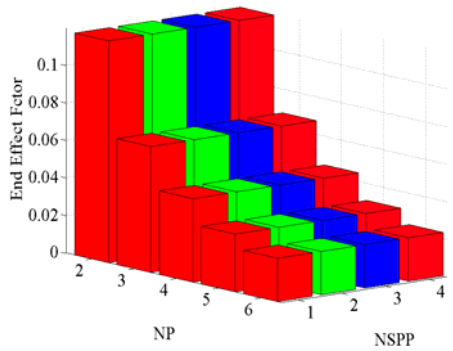

Fig. 7 End effect Intensity versus number of pole pairs and number of slots per pole per phase

The EEF variations related to the frequency and design current density are shown in fig.8. At a constant slip for a constant mechanical speed the decrease in frequency will increase the pole pitch. This causes to a larger secondary time constant and smaller end effect. The design current density has no sensitive effect on end effect intensity. Because in this paper change in design current density only change the slot depth and has no effect on slot width and tooth width.

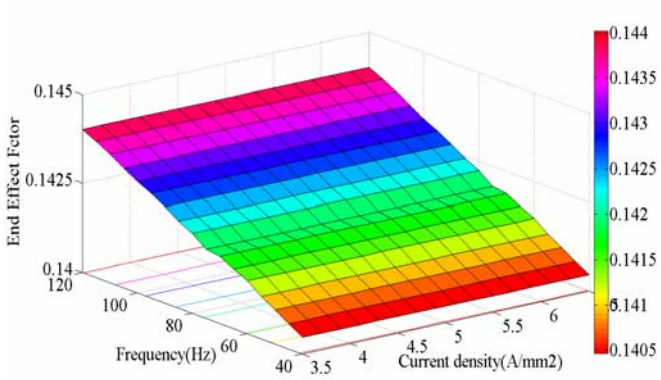

Fig. 8 End effect Intensity versus frequency and current density

Fig.9 shows the variation of EEF by change in the value of slip and primary width to pole pitch ratio. As the slip increase, the end effect intensity will decrease. For a constant frequency to achieve a particular speed slip reduction causes to pole pitch reduction and this decreases the secondary time constant which leads to a more intensive end effect.

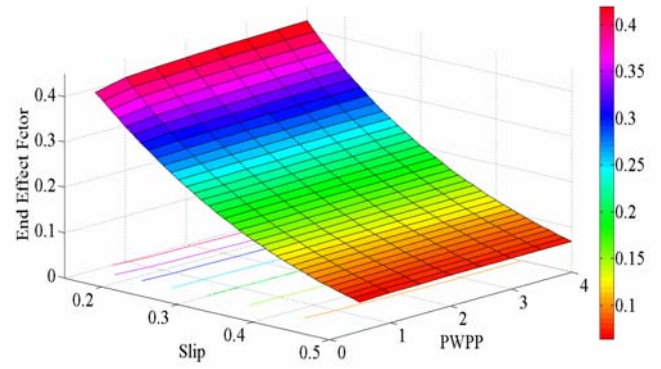

Fig. 9 End effect Intensity versus slip and primary width to pole pitch ratio

V. Validation Stage

This study is carried out based on a new equivalent circuit model. Therefore, validity of the results mainly depends on the accuracy of the circuit model. Thus 2-D time stepping FEM is used to evaluate the results. Fig.10 shows the comparison of results from ECM and FEM. It can be seen that ECM results are close enough to the FEM results.

Fig.11,12 show the flux density distribution, and flux lines, in the SLIM respectively. As the primary of the SLIM moves to right, the flux density reduced in the front of SLIM and reflected behind the SLIM.

Fig.13 shows the flux density distribution in the air gap. It can be seen that the flux density of air gap is less than 0.2T, thus the primary core loss is negligible.

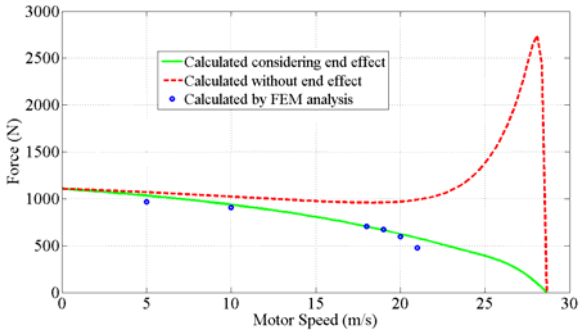

Fig. 10 Force versus speed

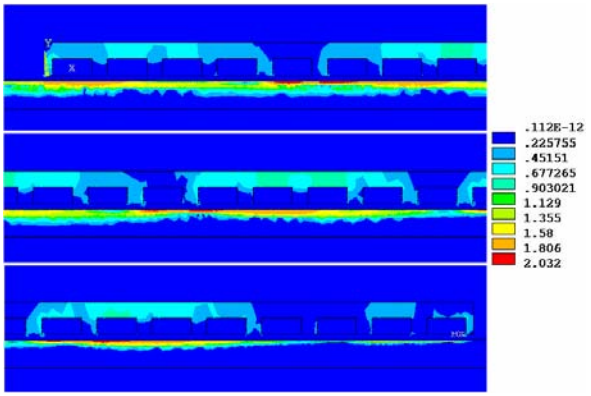

Fig. 11- Flux density distribution in SLIM

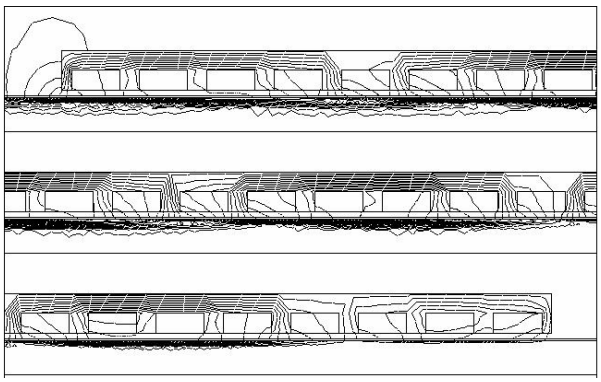

Fig. 12 Flux lines in the SLIM

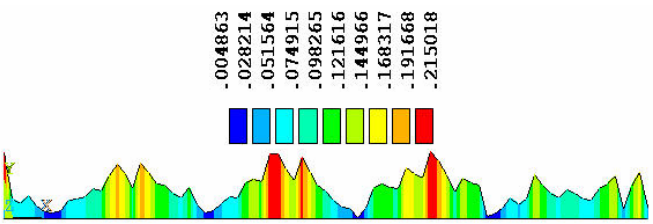

Fig. 13 Flux density distribution in the conducting plate

VI. Conclusion

The paper presents a method to study the influence of design parameters on the end effect intensity in SLIMs. In order to obtain this purpose, a quick equivalent circuit model, was introduced. The model considered the specific phenomena in SLIMs, such as transverse edge effect and saturation effect, by means of some proper factors. The longitudinal end effect was also considered by modifying Duncan's equivalent circuit model. For the purpose of measuring the end effect intensity a new factor, EEF, was introduced. At the end of simulations, the accuracy of suggested ECM was evaluated by 2-D time stepping FEM analysis that implies the good accuracy of this method.

Appendix

Symbols

Symbol	Quantity
W_s, l_{ce}	Stator width and end connection length
P, τ	Number of poles and pole pitch
q	Number of slots per pole per phase
R_1, X_1	Primary resistance and reactance
X_m	Magnetizing reactance
N_{ph}	Number of turns per phase
g_m, d	Air gap length and conducting plate thickness
K_{cp}	Conducting plate coefficient
k_{cp}	Conducting plate coefficient due to edge effect
K_{Fe}	Back iron coefficient
k_{fe}	Back iron coefficient due to edge effect
K_{tr}	Primary to secondary ratio
K_w	Winding factor
K_c, K_l	Carter's coefficient and leakage factor
σ_{cp}, σ_{fe}	Conducting plate and back iron conductivity

References

[1] J. F. Gieras, *Linear Induction Drives*. Oxford, U.K.: New Clarendon Press, 1994.

[2] M. Mirsalim, A. Doroudi,; J.S. Moghani, "Obtaining the operating characteristics of linear induction motors: a new approach" *IEEE Trans. Magn*. Vol.38, pp:1365–1370. Issue:2, March 2002.

[3] J. F. Eastham, "Novel synchronous machines: Linear and disc," *Proc. Inst. Elect. Energ.*, vol. 137, pp. 49–58, Jan. 1990.

[4] T. Koseki , S. Sone, "Investigation of secondary slot pitches of a cage-type linear induction motor," *IEEE Trans. Magn.*, vol. 29, no. 6, pp. 2944–2946, Nov. 1993.

[5] W. Xu, G. Sun, Y, Li,; "Research on Performance Characteristics of Linear Induction Motor" *IEEE Industrial electronics and applications conf*. 2007 pp.86-88.

[6] R.C. Creppe, J.A.C. Ulson, J.F. Rodrigues,; "Influence of Design Parameters on Linear Induction Motor End Effect" *IEEE Trans. Ener.Conv* .vol.23 no.2 pp. 358-362, June. 2008.

[7] K. Idir, G.E. Dawson, A. R. Eastham; "Modeling and Performance of Linear Induction Motor with Saturable Primary" *IEEE Trans. Indus.* vol.29, no.6, pp. 1123-1128, Nov. 1993.

[8] T. Yamaguchi, Y. Kawase, M. Yoshida, Y. Saito; Ohdachi, Y.; "3-D Finite Element Analysis of a Linear Induction Motor" *IEEE Trans. Magn*. vol.37, no.5, pp: 3668-3671. Sep 2001.

[9] Y. Nozaki, T. Koseki, E. Masada; "Analysis of Linear Induction Motors for HSST and Linear Metro using Finite Difference Method" *Proc. of the 5th International Symposium on Linear Drives for Industry Applications*, pp: 168-171, LDIA2005.
[10] N. Fujii , T. Harada, "A New Viewpoint of End Effect of Linear Induction Motor from Secondary Side in Ladder Type Model" *IEEE Trans. Magn.*, vol. 35, no. 5, pp. 4040–4042, Sep. 1993.
[11] A. H. Selçuk , H. Kürüm, "Investigation of End Effects in Linear Induction Motors by Using the Finite-Element Method" *IEEE Trans. Magn.*, vol. 44, no. 7, pp. 1791–1795, July. 2008.
[12] N. Fujii, T. Kayasuga, T. Hoshi, "Simple End Effect Compensator for Linear Induction Motor" *IEEE Trans. Magn.*, vol. 38, no. 5, pp. 3270–3272, Sep. 2002.
[13] R. C. Creppe, J. A. C. Ulson, J. F. Rodrigues, "Influence of Design Parameters on Linear Induction Motor End Effect" *IEEE Energy Conv. Magn.*, vol. 23, no. 2, pp. 3270–3272, June. 2008.
[14] J.H. Sung, K. Nam, "A New Approach to Vector Control for a Linear Induction Motor Considering End Effects," *IEEE IAS annual meeting*, pp.2284-2289, 1999.
[15] J. Duncan, "Linear induction motor—Equivalent circuit model," *Proc. Inst. Elec. Eng.*, pt. B, vol. 130, no. 1, 1983.
[16] J. Faiz, H. Jafari; "Accurate Modeling of Single-Sided Linear Induction Motor Considers End Effect and Equivalent Thickness" *IEEE Trans. Magn.* vol.36, no.5, pp:3785-3790, Sep 2000.
[17] I. Boldea and S. A. Nasar, *Linear Electromagnetic Device.* New York: Taylor & Francis, 2001.
[18] R. M. Pai, I. Boldea, and S. A. Nasar, "A complete equivalent circuit of a linear induction motor with sheet secondary," *IEEE Trans. Magn.*, vol. 24, pp. 639–654, Jan. 1988.